48th AIAA/ASME/ASCE/AHS/ASC Structures, Structural Dynamics, and Materials Con
23-26 April 2007, Honolulu, Hawaii

AIAA 2007-2084

A Critical Evaluation of the Predictive Capabilities of Various Advanced Micromechanics Models

Wenbin Yu*
Utah State University, Logan, Utah 84322-4130
Todd O. Williams†
Los Alamos National Laboratory, Los Alamos, New Mexico 87545
Brett A. Bednarcyk‡
Ohio Aerospace Institute, Cleveland, OH 44142
Jacob Aboudi§
Tel-Aviv University, Ramat-Aviv, Israel
and
Tian Tang¶
Utah State University, Logan, Utah 84322-4130

The focus of this work is to critically evaluate the predictive capabilities of several advanced micromechanics models, including GMC, HFGMC, ECM, and VAMUCH. The comparison concentrates primarily on predictions for the effective elastic properties and local stress fields based on micromechanics approaches for various types of composite systems. Both exact analytical solutions and finite element simulations will be utilized in the comparison to assess the accuracy of the different models. It is found that for some microstructures, most of the compared models provide similar and reliable predictions for effective properties. For an accurate prediction for local stress distributions, HFGMC and VAMUCH significantly outperform GMC, which provides only average local fields. A very challenging X shape microstructure is also proposed in this paper which pushes all the micromechanics models to their limits. This case clearly discloses the fallacy about micromechanics that every model "works" as far as effective properties concerned. Such an assessment can help engineers choose the appropriate micromechanics model for composites they are dealing with in their applications.

Introduction

As structural applications become more demanding it is becoming increasingly important that the fundamental response mechanisms controlling both the microscopic and macroscopic behavior of structural materials be well understood. Properly quantified in a material model such understanding can be used to improve structural designs, make more accurate estimates of a given structure's capabilities, or engineer a material's microstructure in order to enhance desirable performance characteristics.

The fundamental response mechanisms in all heterogeneous materials are driven by the localization processes induced by the presence of the heterogeneities (the microstructures) that exist in these materials. Micromechanical theories are particularly well suited to modeling localization processes and how they influence the micro- and macroscopic material behavior since these theories predict the multiscale material

*Assistant Professor, Department of Mechanical and Aerospace Engineering. Senior Member, AIAA; Member, ASME and AHS.
†Technical Staff Member, Theoretical Division, T-3.
‡Senior Scientist, Member, AIAA.
§Professor, Department of Solid Mechanics, Materials and Structures
¶Graduate Research Assistant, Department of Mechanical and Aerospace Engineering. Student Member, AIAA.

response based directly on a knowledge of the behavior of the individual component materials and of the heterogeneous microstructure.

There are a number of different types of homogenization tools available. The simplest such models,[1,2] which are based on strength of materials assumptions, can only be considered to give very rough estimates for a material's response characteristics. Mean field theories, such as the Mori-Tanaka theory[3,4] can provide reasonable estimates for a material's bulk elastic response but typically fail to provide good estimates for the local responses and the history-dependent responses of the material. In order to correctly predict the local and bulk response characteristics in the elastic and inelastic domains it is necessary to utilize micromechanical theories that consider both the average fields within phases as well as the fluctuating fields within the phases.[5] A set of relatively simple micromechanical models that have attempted to develop such capabilities are the so-call "Method of Cells" (MOC)[6] and the "Generalized Method of Cells" (GMC).[7,8] These approaches are based on the use of average strain and stress fields within discrete subvolumes of the microstructure. A review of some of the published work using these models is given in Ref. 9. One shortcoming of the MOC/GMC models is the lack of coupling between the local shearing and normal responses for composites composed of phases with at least orthotropic symmetry. This lack of coupling has significant implications for predicting the history-dependent behavior of such materials. In order to overcome this lack of coupling in the local fields it is necessary to utilize theories with more accurate representations of the local fields. There are a number of such theories currently available. Two very different approaches that have been developed in an attempt to directly address the lack of coupling in the MOC/GMC set of models are the so-called "High Fidelity Generalized Method of Cells" (HFGMC) model[10] and the so-called "Elasticity-based Cell Model".[5,11,12] Obviously, various other models that exhibit (potentially) accurate representations of the microfields in the composite exist which have no connection to the original MOC/GMC methodologies. Examples of such theories are Green's function based analyses[13] and asymptotic homogenization approaches.[14] A recently developed variant of the asymptotic homogenization approach is the Variational Asymptotic Method for Unit Cell Homogenization (VAMUCH).[15–17] In contrast to conventional asymptotic methods, VAMUCH carries out an asymptotic analysis of the variational statement, synthesizing the merits of both variational methods and asymptotic methods. Finally, there are a number of purely numerical approaches, such as finite element analyses,[18,19] and particle-in-cell methods,[20] that have been used to model the micromechanical response of heterogeneous materials.

Obviously, significant effort has been expended to develop a number of approaches that can be used to consider the micromechanical responses of composite systems. However, there has been relatively little work done that compares the predictive capabilities of different approaches. One such study, carried out by Lissenden and Herakovich,[21] considered the ability of various simplified micromechanical theories to predict the bulk elastic properties of continuous fiber composites. However, in today's environment of advanced applications it is no longer sufficient to consider only the predictions for the bulk characteristics. It is now necessary to consider the predictive capabilities for the local fields within the material system.

The focus of the current work is the comparison of the predictive capabilities of several advanced micromechanical theories; the GMC theory, the HFGMC theory, the ECM theory, and VAMUCH, with each other as well as with established analytical solutions and finite element predictions. The work will consider both the local and global responses. Since accurate predictions for the elastic fields within the composite are a necessary prerequisite for accurately predicting the history-dependent behavior of heterogeneous materials the current comparisons focus on the elastic predictions.

The Generalized Method of Cells (GMC)

The starting point for the GMC theory is the discretization of the periodic material microstructure into rectangular (for the two-dimensional (2D) theory) or rectilinear parallelepiped (for the three-dimensional (3D) theory) subregions; see Fig. 1. Each of these subregions is termed a subcell. The displacement field within each subcell is modeled using the representation (for 3D microstructures)

$$u_i^{(\alpha,\beta,\gamma)} = \Psi_i^{(\alpha,\beta,\gamma)}\overline{x}_1 + \Gamma_i^{(\alpha,\beta,\gamma)}\overline{x}_2 + \Omega_i^{(\alpha,\beta,\gamma)}\overline{x}_3 \tag{1}$$

This displacement field representation results in uniform strains within each subcell (although the strains in different subcells are typically different).

Satisfaction of the displacement continuity conditions between subcells as well as between repeating material volumes, either unit cells (UC) or representative volume elements (RVEs), gives the following set

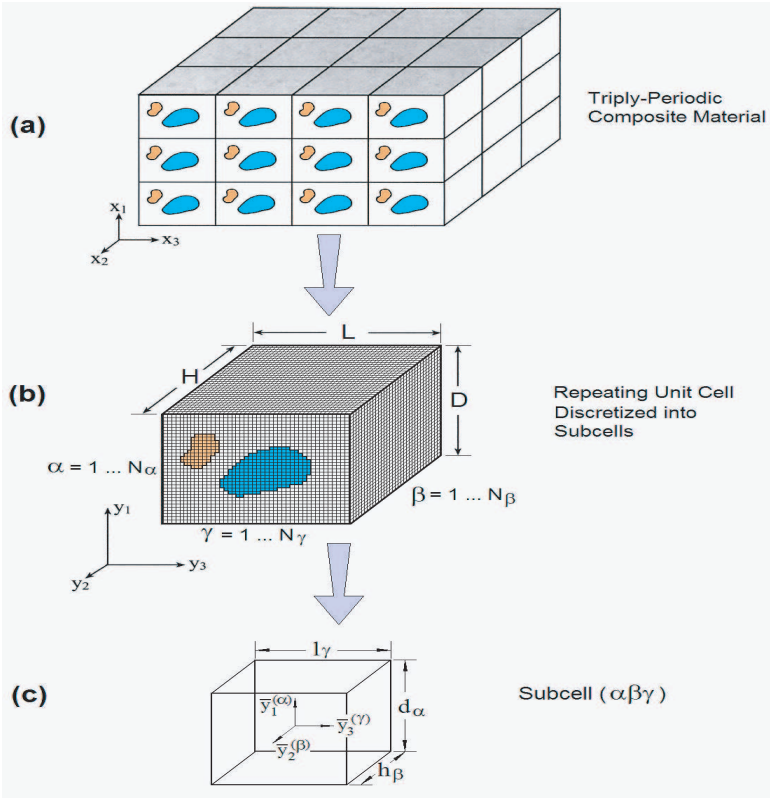

Figure 1. The discretized repeating volume for a particulate composite used by the original GMC model, the HFGMC theory, and the ECM.

of governing equations

$$
\begin{aligned}
\sum_{\alpha=1}^{N_\alpha} d_\alpha \Psi_1^{(\alpha,\beta,\gamma)} &= \left(\sum_{\alpha=1}^{N_\alpha} d_\alpha\right) \bar{\epsilon}_{11} \\
\sum_{\beta=1}^{N_\beta} h_\beta \Gamma_2^{(\alpha,\beta,\gamma)} &= \left(\sum_{\beta=1}^{N_\beta} h_\beta\right) \bar{\epsilon}_{22} \\
\sum_{\gamma=1}^{N_\gamma} l_\gamma \Omega_3^{(\alpha,\beta,\gamma)} &= \left(\sum_{\gamma=1}^{N_\gamma} l_\gamma\right) \bar{\epsilon}_{33} \\
\sum_{\beta=1}^{N_\beta}\sum_{\gamma}^{N_\gamma} h_\beta l_\gamma \epsilon_{23}^{(\alpha,\beta,\gamma)} &= \left(\sum_{\beta=1}^{N_\beta}\sum_{\gamma}^{N_\gamma} h_\beta l_\gamma\right) \bar{\epsilon}_{23} \\
\sum_{\alpha=1}^{N_\alpha}\sum_{\gamma}^{N_\gamma} d_\alpha l_\gamma \epsilon_{13}^{(\alpha,\beta,\gamma)} &= \left(\sum_{\alpha=1}^{N_\alpha}\sum_{\gamma}^{N_\gamma} d_\alpha l_\gamma\right) \bar{\epsilon}_{13} \\
\sum_{\alpha=1}^{N_\alpha}\sum_{\beta}^{N_\beta} d_\alpha h_\beta \epsilon_{12}^{(\alpha,\beta,\gamma)} &= \left(\sum_{\alpha=1}^{N_\alpha}\sum_{\beta}^{N_\beta} d_\alpha h_\beta\right) \bar{\epsilon}_{12}
\end{aligned}
\tag{2}
$$

where $\overline{\epsilon}_{ij}$ are the applied average strain field and where

$$\begin{aligned}
\epsilon_{23}^{(\alpha,\beta,\gamma)} &= \left(\Omega_2^{(\alpha,\beta,\gamma)} + \Gamma_3^{(\alpha,\beta,\gamma)}\right)/2 \\
\epsilon_{13}^{(\alpha,\beta,\gamma)} &= \left(\Omega_1^{(\alpha,\beta,\gamma)} + \Psi_3^{(\alpha,\beta,\gamma)}\right)/2 \\
\epsilon_{12}^{(\alpha,\beta,\gamma)} &= \left(\Psi_2^{(\alpha,\beta,\gamma)} + \Gamma_1^{(\alpha,\beta,\gamma)}\right)/2
\end{aligned} \tag{3}$$

Satisfaction of the traction continuity conditions in an average sense between subcells as well as between repeating material volumes gives the following governing relations

$$\begin{aligned}
&\sigma_{11}^{(\alpha,\beta,\gamma)} = \sigma_{11}^{(\alpha+1,\beta,\gamma)} && \text{for } \alpha = 1,..,N_\alpha - 1, \beta = 1,..,N_\beta, \gamma = 1,..,N_\gamma \\
&\sigma_{22}^{(\alpha,\beta,\gamma)} = \sigma_{22}^{(\alpha,\beta+1,\gamma)} && \text{for } \alpha = 1,..,N_\alpha, \beta = 1,..,N_\beta - 1, \gamma = 1,..,N_\gamma \\
&\sigma_{33}^{(\alpha,\beta,\gamma)} = \sigma_{33}^{(\alpha,\beta,\gamma+1)} && \text{for } \alpha = 1,..,N_\alpha, \beta = 1,..,N_\beta, \gamma = 1,..,N_\gamma - 1 \\
&\sigma_{23}^{(\alpha,\beta,\gamma)} = \sigma_{23}^{(\alpha,\beta,\gamma+1)} && \text{for } \alpha = 1,..,N_\alpha, \beta = 1,..,N_\beta - 1, \gamma = 1,..,N_\gamma \\
&\sigma_{23}^{(\alpha,\beta,\gamma)} = \sigma_{23}^{(\alpha,\beta+1,\gamma)} && \text{for } \alpha = 1,..,N_\alpha, \beta = N_\beta, \gamma = 1,...,N_\gamma - 1 \\
&\sigma_{13}^{(\alpha,\beta,\gamma)} = \sigma_{13}^{(\alpha,\beta,\gamma+1)} && \text{for } \alpha = 1,..,N_\alpha - 1, \beta = 1,..,N_\beta, \gamma = 1,..,N_\gamma \\
&\sigma_{13}^{(\alpha,\beta,\gamma)} = \sigma_{13}^{(\alpha+1,\beta,\gamma)} && \text{for } \alpha = N_\alpha - 1, \beta = 1,..,N_\beta, \gamma = 1,...,N_\gamma - 1 \\
&\sigma_{12}^{(\alpha,\beta,\gamma)} = \sigma_{12}^{(\alpha,\beta+1,\gamma)} && \text{for } \alpha = 1,..,N_\alpha - 1, \beta = 1,..,N_\beta, \gamma = 1,..,N_\gamma \\
&\sigma_{12}^{(\alpha,\beta,\gamma)} = \sigma_{12}^{(\alpha+1,\beta,\gamma)} && \text{for } \alpha = N_\alpha, \beta = 1,...,N_\beta - 1, \gamma = 1,..,N_\gamma
\end{aligned} \tag{4}$$

The above system of governing equations can be cast in the following matrix form

$$\tilde{A}\epsilon_s - \tilde{D}\left(\epsilon_s^I + \epsilon_s^T\right) = K\overline{\epsilon} \tag{5}$$

Solving Eqn. (5) for the subcell strains ϵ_s yields

$$\epsilon_s = A\overline{\epsilon} + D\left(\epsilon_s^I + \epsilon_s^T\right) \tag{6}$$

where A and D are the mechanical and eigenstrain concentration tensors, respectively.

The bulk constitutive relations for the composite

$$\overline{\sigma} = B^*\left(\overline{\epsilon} - \overline{\epsilon}^I - \overline{\epsilon}^T\right) \tag{7}$$

are obtained by substituting Eqn. (6) into the average stress theorem. Explicit expressions for the terms B^*, $\overline{\epsilon}^I$, and $\overline{\epsilon}^T$ are give in Ref. 8.

There are a couple of characteristics in the GMC theory that should be kept in mind. First, as mentioned previously there is no geometrically induced coupling between the local normal and shearing effects. Additionally, there is no geometrically induced coupling between the local shearing effects. Since the stresses in each subcell are spatially uniform within the subcell every subcell along a given row of subcells (in any of the directions) experiences the same stress along that direction. Furthermore, the behavior along the row is typically dominated by the most compliant material in the row. These characteristics of the GMC approach were utilized in Refs. 22 and 23 to reformulate the 2D and 3D versions of GMC, respectively, in order to maximize the computational efficiency of the method (i.e., minimize the number of unknown variables). For full details of the GMC formulation for see Ref. 7 for 2D UCs and Ref. 8 for 3D UCs.

The High-Fidelity Generalized Method of Cells Theory (HFGMC)

The version of HFGMC that is described herein is designated for the prediction of the effective thermoinelastic behavior of composites with discontinuous fibers (i.e., short-fiber composites). This three-dimensional, triply periodic theory has been fully described in Ref. 10 in the case of linear electro-magneto-thermo-elastic materials. Thus, thermoelastic phases can by obtained as a special case. The inclusion of inelastic effects in the phases follows the analysis that has been presented in Ref. 24 in the two-dimensional case of continuous fibers. This micromechanical model is briefly outlined in the following.

This model is based on a homogenization technique for composites with periodic microstructure as shown in Fig. 1(a) in terms of the global coordinates (x_1, x_2, x_3). The parallelepiped repeating unit cell, Fig. 1(b), defined with respect to the local coordinates (y_1, y_2, y_3), of such a composite is divided into N_α, N_β, and N_γ subcells, in the y_1, y_2, and y_3 directions, respectively. Each subcell is labeled by the indices (α, β, γ) with $\alpha = 1, ..., N_\alpha$, $\beta = 1, ..., N_\beta$, and $\gamma = 1, ..., N_\gamma$, and may contain a distinct homogeneous material. The dimensions of the subcell are denoted by d_α , h_β , and l_γ, respectively. A local coordinate system, $(\overline{y}_1^{(\alpha)}, \overline{y}_2^{(\beta)}, \overline{y}_3^{(\gamma)})$ is introduced in each subcell whose origin is located at the subcell center. The local (subcell) constitutive equation of the material which, in general, is assumed to be thermoinelastic, is given by

$$\sigma^{(\alpha,\beta,\gamma)} = C^{(\alpha,\beta,\gamma)} \left(\epsilon^{(\alpha,\beta,\gamma)} - \epsilon^{I(\alpha,\beta,\gamma)} \right) - \Gamma^{(\alpha,\beta,\gamma)} \Delta T \tag{8}$$

where $\sigma^{(\alpha,\beta,\gamma)}$, $\epsilon^{(\alpha,\beta,\gamma)}$, $\epsilon^{I(\alpha,\beta,\gamma)}$, and $\Gamma^{(\alpha,\beta,\gamma)}$ are the stress, total strain, inelastic strain and thermal stress tensors, respectively, in subcell (α, β, γ), $C^{(\alpha,\beta,\gamma)}$ is the stiffness tensor of the material in the subcell (α, β, γ), and ΔT denotes the temperature deviation from a reference temperature.

The basic assumption in HFGMC is that the displacement vector $u^{(\alpha,\beta,\gamma)}$ in each subcell is expanded into quadratic form in terms of its local coordinates $(\overline{y}_1^{(\alpha)}, \overline{y}_2^{(\beta)}, \overline{y}_3^{(\gamma)})$ as follows

$$\begin{aligned} u^{(\alpha,\beta,\gamma)} = \; & \bar{\epsilon} x + W_{(000)}^{(\alpha,\beta,\gamma)} + \overline{y}_1^{(\alpha)} W_{(100)}^{(\alpha,\beta,\gamma)} + \overline{y}_2^{(\beta)} W_{(010)}^{(\alpha,\beta,\gamma)} + \overline{y}_3^{(\gamma)} W_{(001)}^{(\alpha,\beta,\gamma)} \\ & + \frac{1}{2} \left(3\overline{y}_1^{(\alpha)2} - \frac{d_\alpha^2}{4} \right) W_{(200)}^{(\alpha,\beta,\gamma)} + \frac{1}{2} \left(3\overline{y}_2^{(\beta)2} - \frac{h_\beta^2}{4} \right) W_{(020)}^{(\alpha,\beta,\gamma)} + \frac{1}{2} \left(3\overline{y}_3^{(\gamma)2} - \frac{l_\gamma^2}{4} \right) W_{(002)}^{(\alpha,\beta,\gamma)} \end{aligned} \tag{9}$$

where $\bar{\epsilon}$ is the applied (external) average strain, and the unknown terms $W_{(kmn)}^{(\alpha,\beta,\gamma)}$ must be determined from the fulfillment of the equilibrium conditions, the periodic boundary conditions, and the interfacial continuity conditions of displacements and tractions between subcells. The periodic boundary conditions ensure that the displacements and tractions at opposite surfaces of the repeating unit cell are identical, see Ref. 10 for more details. A principal ingredient in this micromechanical analysis is that all these conditions are imposed in the average (integral) sense.

Note that GMC employs a first order expansion of the displacement vector in the subcell (see Eqn. (1)). The second order expansion in Eqn. (9) for HFGMC has been previously employed in the analysis of wave propagation in composite materials,[25–27] and in the determination of the response of functionally graded materials to thermoelastic loading.[28]

As a result of the imposition of the equilibrium equations in the subcells together with the application of the interfacial and periodicity conditions, a linear system of algebraic equations is obtained which can be represented in the following form

$$KU = f + g \tag{10}$$

where the matrix K contains information on the geometry and thermomechanical properties of the materials within the individual subcells (α, β, γ), and the displacement vector U contains the unknown displacement coefficients $W_{(kmn)}^{(\alpha,\beta,\gamma)}$ in Eqn. (9), f is a vector containing information on the applied average strains $\bar{\epsilon}$ and the imposed temperature deviation ΔT, and g is a vector containing the inelastic effects given in terms of the integrals of the inelastic strain distributions. These integrals depend implicitly on the elements of the displacement coefficient vector U, requiring an incremental solution of Eqn. (10) at each point along the loading path, see Ref. 24 for more details. Eqn. (10) forms a system of $21 N_\alpha N_\beta N_\gamma$ algebraic equations. Computational efficiency issues related to solving these equations within the HFGMC are discussed in Ref. 29.

The solution of Eqn. (10) enables the establishment of the following localization relation which expresses the average strain $\bar{\epsilon}^{(\alpha,\beta,\gamma)}$ in the subcell (α, β, γ) to the externally applied average $\bar{\epsilon}$, which are given in Ref. 30 as

$$\bar{\epsilon}^{(\alpha,\beta,\gamma)} = A^{(\alpha,\beta,\gamma)} \bar{\epsilon} + A^{th(\alpha,\beta,\gamma)} \Delta T + D^{I(\alpha,\beta,\gamma)} \tag{11}$$

where $A^{(\alpha,\beta,\gamma)}$ and $A^{th(\alpha,\beta,\gamma)}$ are the mechanical and thermal strain concentration tensors, respectively, of the subcell (α, β, γ), and $D^{I(\alpha,\beta,\gamma)}$ is a vector that involves the current inelastic effects in the subcell.

The final form of the effective constitutive law of the multiphase thermo-inelastic composite, which relates the average stress $\overline{\sigma}$ and strain $\bar{\epsilon}$, is established as follows:

$$\overline{\sigma} = C^* \bar{\epsilon} - \left(\Gamma^* \Delta T + \overline{\sigma}^I \right) \tag{12}$$

In this equation C^* is the effective stiffness tensor and Γ^* is the effective thermal stress tensor of the composite, and $\overline{\sigma}^I$ is the global inelastic stress tensor. All of these global quantities can be expressed in a closed-form manner in terms of the mechanical and thermal concentration tensors which appear in Eqn. (11) together with the inelastic term $D^{I(\alpha,\beta,\gamma)}$, which are given in Ref. 30 as follows

$$C^* = \frac{1}{DHL}\sum_{\alpha=1}^{N_\alpha}\sum_{\beta=1}^{N_\beta}\sum_{\gamma=1}^{N_\gamma} d_\alpha h_\beta l_\gamma C^{(\alpha,\beta,\gamma)} A^{(\alpha,\beta,\gamma)}$$

$$\Gamma^* = -\frac{1}{DHL}\sum_{\alpha=1}^{N_\alpha}\sum_{\beta=1}^{N_\beta}\sum_{\gamma=1}^{N_\gamma} d_\alpha h_\beta l_\gamma \left(C^{(\alpha,\beta,\gamma)} A^{th(\alpha,\beta,\gamma)} - \Gamma^{(\alpha,\beta,\gamma)}\right)$$

$$\overline{\sigma}^I = -\frac{1}{DHL}\sum_{\alpha=1}^{N_\alpha}\sum_{\beta=1}^{N_\beta}\sum_{\gamma=1}^{N_\gamma} d_\alpha h_\beta l_\gamma \left(C^{(\alpha,\beta,\gamma)} D^{I(\alpha,\beta,\gamma)} - R_{(000)}^{(\alpha,\beta,\gamma)}\right) \tag{13}$$

where $R_{(000)}^{(\alpha,\beta,\gamma)}$ is an expression that represents the integral of the inelastic strain distributions.

Based on the generalized method of cells family of models, the NASA Glenn Research Center developed a micromechanics computer code, referred to as MAC/GMC, that has many user-friendly features and significant flexibility for the analysis of continuous, discontinuous, and woven polymer, ceramic, and metal matrix composites with phases that can be represented by arbitrary elastic, viscoelastic, and/or viscoplastic constitutive models. The most recent version of a user guide to this code (version 4) which has been presented by Bednarcyk and Arnold[31] incorporates HFGMC, together with additional material models including smart materials (electromagnetic and shape memory alloys) and yield surface prediction of metal matrix composites.

The Elasticity-Based Cell Model (ECM)

The Elasticity-Based Cell Model (ECM)[5,11,12] starts with the same type of microstructural discretization as used by the original GMC theory, Fig. 1. The displacement field within each subcell is given in terms of an infinite series

$$u_i^{(\alpha_1,\alpha_2,\alpha_3)}\left(\underline{x},\underline{y}\right) = \overline{\epsilon}_{ij}x_j + P_{(o_1,o_2,o_3)}^{(\alpha_1,\alpha_2,\alpha_3)}\left(\underline{y}\right) V_{i(o_1,o_2,o_3)}^{(\alpha_1,\alpha_2,\alpha_3)} \tag{14}$$

where the $\overline{\epsilon}_{ij}$ are the components of the bulk strain field, the x_j are the macroscopic coordinate components, $P_{(o_1,o_2,o_3)}^{(\alpha_1,\alpha_2,\alpha_3)}\left(\underline{y}\right) = p_{(o_1)}^{(\alpha_1)}(y_1)p_{(o_2)}^{(\alpha_2)}(y_2)p_{(o_3)}^{(\alpha_3)}(y_3)$ and the $p_{(o_i)}$ are orthogonal polynomial terms of order o_i in the y_i (the local coordinate) directions in the subcells. The corresponding subcell strain and stress fields are given by

$$\begin{aligned}\epsilon_{ij}^{(\alpha_1,\alpha_2,\alpha_3)} &= P_{(0,0,0)}^{(\alpha_1,\alpha_2,\alpha_3)}\overline{\epsilon}_{ij} + P_{(o_1,o_2,o_3)}^{(\alpha_1,\alpha_2,\alpha_3)}\mu_{ij(o_1,o_2,o_3)}^{(\alpha_1,\alpha_2,\alpha_3)}\\ \sigma_{ij}^{(\alpha_1,\alpha_2,\alpha_3)} &= P_{(o_1,o_2,o_3)}^{(\alpha_1,\alpha_2,\alpha_3)}\sigma_{ij(o_1,o_2,o_3)}^{(\alpha_1,\alpha_2,\alpha_3)}\end{aligned} \tag{15}$$

The $\mu_{ij(o_1,o_2,o_3)}^{(\alpha_1,\alpha_2,\alpha_3)}$ represent the fluctuating strain effects. Summation on repeated order indices, o_i, is assumed.

Making use of the orthogonality properties of the expansions functions the equilibrium equations are satisfied by

$$\sigma_{1j(o_1',o_2,o_3)}^{(\alpha_1,\alpha_2,\alpha_3)} a_{(o_1',o_1)}^{(\alpha_1)} + \sigma_{2j(o_1,o_2',o_3)}^{(\alpha_1,\alpha_2,\alpha_3)} a_{(o_2',o_2)}^{(\alpha_2)} + \sigma_{3j(o_1,o_2,o_3')}^{(\alpha_1,\alpha_2,\alpha_3)} a_{(o_3',o_3)}^{(\alpha_1)} = 0 \tag{16}$$

which results in pointwise satisfaction of the equilibrium conditions.

Imposing traction continuity in terms of the different expansion orders within the subcell surfaces (both between subcells within a repeating volume as well as between repeating volumes) gives

$$\begin{aligned}\sigma_{1i(o_1,o_2,o_3)}^{(\alpha_1,\alpha_2,\alpha_3)} p_{o_1}^{(\alpha_1)}\left(\delta_{(1)}^{(\alpha_1)}\right) &= \sigma_{1i(o_1,o_2,o_3)}^{(\tilde{\alpha}_1,\alpha_2,\alpha_3)} p_{o_1}^{(\tilde{\alpha}_1)}\left(-\delta_{(1)}^{(\tilde{\alpha}_1)}\right)\\ \sigma_{2i(o_1,o_2,o_3)}^{(\alpha_1,\alpha_2,\alpha_3)} p_{o_2}^{(\alpha_2)}\left(\delta_{(2)}^{(\alpha_2)}\right) &= \sigma_{2i(o_1,o_2,o_3)}^{(\alpha_1,\tilde{\alpha}_2,\alpha_3)} p_{o_2}^{(\tilde{\alpha}_2)}\left(-\delta_{(2)}^{(\tilde{\alpha}_2)}\right)\\ \sigma_{3i(o_1,o_2,o_3)}^{(\alpha_1,\alpha_2,\alpha_3)} p_{o_3}^{(\alpha_3)}\left(\delta_{(3)}^{(\alpha_3)}\right) &= \sigma_{3i(o_1,o_2,o_3)}^{(\alpha_1,\alpha_2,\tilde{\alpha}_3)} p_{o_3}^{(\tilde{\alpha}_3)}\left(-\delta_{(3)}^{(\tilde{\alpha}_3)}\right)\end{aligned} \tag{17}$$

where $\delta_{(i)}^{(\alpha_i)} = d_{(i)}^{\alpha_i}/2$. As was the case for the equilibrium conditions the above equations represent pointwise satisfaction of the interfacial traction continuity constraints.

Following similar procedures to those used to obtain the traction continuity equations, the displacement continuity conditions at the different interfaces are seen to be satisfied by

$$\begin{aligned}
p_{o_1}^{(\alpha_1)}\left(\delta_{(1)}^{(\alpha_1)}\right) V_{i(o_1,o_2,o_3)}^{(\alpha_1,\alpha_2,\alpha_3)} &= p_{o_1}^{(\tilde{\alpha}_1)}\left(-\delta_{(1)}^{(\tilde{\alpha}_1)}\right) V_{i(o_1,o_2,o_3)}^{(\tilde{\alpha}_1,\alpha_2,\alpha_3)} \\
p_{o_2}^{(\alpha_2)}\left(\delta_{(2)}^{(\alpha_2)}\right) V_{i(o_1,o_2,o_3)}^{(\alpha_1,\alpha_2,\alpha_3)} &= p_{o_2}^{(\tilde{\alpha}_2)}\left(-\delta_{(2)}^{(\tilde{\alpha}_2)}\right) V_{i(o_1,o_2,o_3)}^{(\alpha_1,\tilde{\alpha}_2,\alpha_3)} \\
p_{o_3}^{(\alpha_3)}\left(\delta_{(3)}^{(\alpha_3)}\right) V_{i(o_1,o_2,o_3)}^{(\alpha_1,\alpha_2,\alpha_3)} &= p_{o_3}^{(\tilde{\alpha}_3)}\left(-\delta_{(3)}^{(\tilde{\alpha}_3)}\right) V_{i(o_1,o_2,o_3)}^{(\alpha_1,\alpha_2,\tilde{\alpha}_3)}
\end{aligned} \tag{18}$$

for $\alpha_i = 1, .., N_i$. The above forms of the interfacial displacement conditions result in pointwise satisfaction of these constraints.

Once a set of constitutive relations for the phases has been specified the above set of governing equations can be directly expressed in terms of the fundamental kinematic unknowns, $V_{i(o_1,o_2,o_3)}^{(\alpha_1,\alpha_2,\alpha_3)}$. A sufficiently general form for the history-dependent constitutive relations relating the subcell stress and strain fields is given by

$$\sigma_{ij} = L_{ijkl}\epsilon_{kl} + \lambda_{ij} \tag{19}$$

where the L_{ijkl} are the material stiffness components and the λ_{ij} are the eigenstresses which represent the evolving history-dependent response of a material. The forms of the governing equations based on the above constitutive form are not given here for conciseness (see Ref. [5] for these details).

The above system of governing equations can be cast in the form

$$BV = \hat{A}\bar{\epsilon} + F\lambda \tag{20}$$

which in turn can be solved for the concentration tensors to give

$$\mu^{(\alpha_1,\alpha_2,\alpha_3)} = A^{(\alpha_1,\alpha_2,\alpha_3)}\bar{\epsilon} + F^{(\alpha_1,\alpha_2,\alpha_3|\beta_1,\beta_2,\beta_3)}\lambda^{(\beta_1,\beta_2,\beta_3)} \tag{21}$$

For the full details of the ECM formulation (both infinite series and general truncated expansions) see Ref. [5]. The formulations for specialized microstructures are given in Refs. [11, 12].

The Variational Asymptotic Method for Unit Cell Homogenization (VAMUCH)

Recently, a new micromechanics model, the Variational Ssymptotic Method for Unit Cell Homogenization (VAMUCH),[15–17] has been developed by invoking three assumptions: 1) size of the microstructure is much smaller than the macroscopic size of the material; 2) exact solutions of the field variables have volume averages over the UC; 3) effective material properties are independent of macroscopic geometry, boundary and loading conditions of the structure.

The derivation of VAMUCH starts from a variational statement of the heterogenous continuum. Taking advantage of the smallness of the microstructure, one can formulate the homogenization problem as a constrained minimization problem posed over a single UC by carrying out an asymptotic analysis of the variational statement. The final theory of VAMUCH for homogenizing elastic materials can be obtained by minimizing

$$\Pi_\Omega = \frac{1}{2\Omega}\int_\Omega C_{ijkl}\left[\bar{\epsilon}_{ij} + \chi_{(i|j)}\right]\left[\bar{\epsilon}_{kl} + \chi_{(k|l)}\right] \mathrm{d}\Omega \tag{22}$$

subject to the following constraints

$$\chi_i(\mathbf{x}; d_1/2, y_2, y_3) = \chi_i(\mathbf{x}; -d_1/2, y_2, y_3) \tag{23}$$

$$\chi_i(\mathbf{x}; y_1, d_2/2, y_3) = \chi_i(\mathbf{x}; y_1, -d_2/2, y_3) \tag{24}$$

$$\chi_i(\mathbf{x}; y_1, y_2, d_3/2) = \chi_i(\mathbf{x}; y_1, y_2, -d_3/2) \tag{25}$$

$$\langle\chi_i\rangle = 0 \tag{26}$$

where Eqs. (23)-(25) are the well-known periodic boundary conditions and Eqn. (26) helps uniquely determine the fluctuation functions χ_i. Following the regular steps of calculus of variations, one can easily show that the Euler-Lagrange equations corresponding to this constrained minimization problem are the same as the Mathematical Homogenization Theories (MHT).[15] Although VAMUCH can achieve the same accuracy of MHT, VAMUCH is different from MHT in at least the following three aspects:

- The periodic boundary conditions are derived in VAMUCH, while they are assumed *a priori* in MHT.
- The fluctuation functions are determined uniquely in VAMUCH due to Eq. (26), while they can only be determined up to a constant in MHT.
- VAMUCH has an inherent variational nature which is convenient for numerical implementation, while virtual quantities should be carefully chosen to make MHT variational.[32]

This constrained minimization problem can be solved analytically for very simple cases such as binary composites.[15] For general cases we need to turn to computational techniques for numerical solutions. Since VAMUCH theory is variational, the finite element method is a natural choice as a method to solve this problem. The details of finite element implementation are given in Ref. [16]. As the result, a companion code VAMUCH has been developed as a general-purpose micromechanical analysis code. Although VAMUCH has all the versatility of the finite element method, it is by no means the traditional displacement-base finite element analysis. The code VAMUCH has the following distinctive features:

- No external load is necessary to perform the simulation and the complete set of material properties can be predicted within one analysis.
- The fluctuation functions and local displacements can be determined uniquely;
- The effective material properties and recovered local fields are calculated directly with the same accuracy of the fluctuation functions. No postprocessing type calculations such as averaging stresses and averaging strains are needed
- The dimensionality of the problem is determined by that of the periodicity of the UC. A complete 6×6 effective material matrix can be obtained even for a 1D unit cell.

For details of VAMUCH theory and implementation, please refer to Refs. [15–17].

Case Studies

These micromechanics models will be used to predict the bulk and local elastic responses of various types of fiber reinforced composites. The resulting predictions will be compared to assess the accuracy with which the different models are capable of predicting the local fields as well as the effective bulk properties of different composite systems. For the purpose of comparison, we also use a finite element based micromechanics approach (which is denoted as FEM) proposed by Sun and Vaidya.[18] This method performs the conventional stress analysis of a representative volume element by applying periodic and symmetric boundary conditions. In this work, we used ANSYS to perform all the needed finite element analysis. Using this approach, only the transverse shear moduli G_{23} can be calculated using 2D analysis, and all the other effective properties are calculated using 3D analysis. However, all the other micromechanics models reviewed in the previous section only require a 2D analysis for fiber reinforced composites.

A. Case 1: Eshelby problem

The first case is the Eshelby problem[33] which deals with an isotropic circular fiber embedded in an infinite isotropic matrix subjected to the uniform far-field stress σ_{22}^{∞}. It is a plane strain elasticity problem and can be solved exactly. Although this is not a micromechanics problem because no repeating UCs can be identified in the material, we can consider a material with repeating UCs which have sufficiently small fiber volume fraction (we choose 1% for this example) so that the interaction effects due to the presence of adjacent cells are negligible. Except for this restriction, the exact solution provides an excellent benchmark for validation of the accuracy of the local fields predicted by different micromechanics models.

For calculation, we choose the fiber to be boron with Young's modulus $E = 400.0$ GPa and Poisson's ratio $\nu = 0.20$, the matrix to be epoxy with Young's modulus $E = 3.50$ GPa and Poisson's ratio $\nu = 0.35$. The choice of these materials produces a high elastic moduli mismatch and thus a significant disturbance in the stress field along the interface between fiber and matrix. To obtain the stress distribution within the UC using micromechanics approaches, we need to calculate the effective properties first, which are listed in Table 1. It can be observed that except for GMC, which slightly under predicts the moduli (E_{22}, G_{12}, G_{23})

Table 1. Effective properties of boron/epoxy composites for Eshelby problem

Models	E_{11} (MPa)	E_{22} (MPa)	G_{12} (MPa)	G_{23} (MPa)	ν_{12}	ν_{23}
GMC	7465	3785	1311	1309	0.3484	0.4435
HFGMC	7466	3801	1322	1317	0.3481	0.4424
ECM (5th order)	7466	3793	1315	1313	0.3482	0.4431
VAMUCH	7466	3801	1322	1317	0.3481	0.4424
FEM	7466	3801	1322	1317	0.3481	0.4424

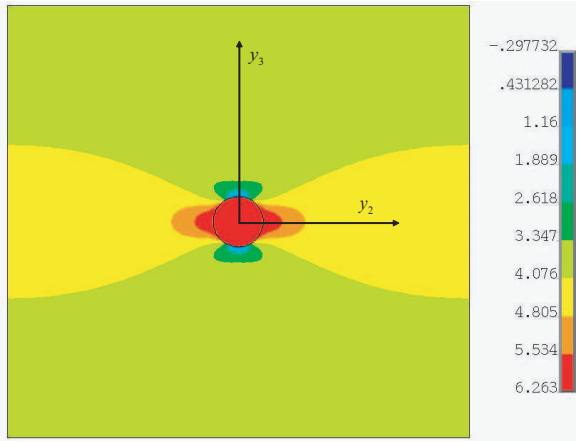

Figure 2. Contour plot of σ_{22} (MPa)

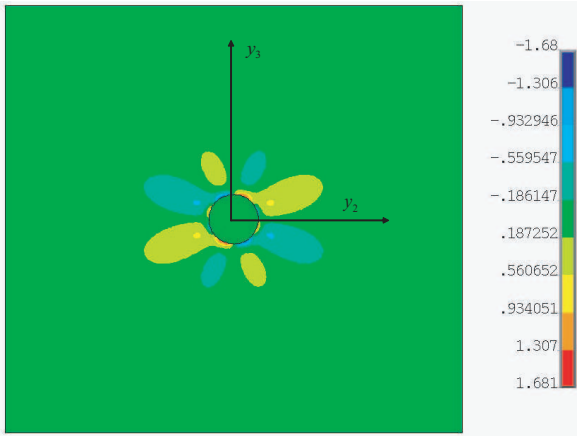

Figure 3. Contour plot of σ_{23} (MPa)

and over predicts the Poisson's ratios, all the other approaches obtain the same results up to the fourth significant figure.

Next we can use these properties to solve the plane strain problem of the effective, homogenized medium under the application of a far-field stress σ_{22}^{∞}, which will generate a macroscopic strain field $\bar{\epsilon}_{22} = 0.1\%$ and corresponding $\bar{\epsilon}_{33}$ due to Possion's effect. Such values can be fed back to the micromechanics models to recover the stress distribution within the material. Figures 2 and 3 show the contour plots for the distributions of σ_{22} and σ_{23} directly obtained using the exact solution, in which the stress concentrations along the interface between fiber and matrix can be clearly observed. Although contour plots can provide us some qualitative information, to rigorously assess the accuracy of micromechanics approaches, we plot σ_{22} distributions predicted by micromechanics approaches (GMC, HFGMC, and VAMUCH) and the exact solution along the lines $y_2 = 0$ and $y_3 = 0$ in Figure 4 and Figure 5, respectively. It is evident that GMC is not predictive for the local field, yet HFGMC and VAMUCH have excellent agreements with the exact solution except that the predictions of HFGMC for the stress field inside the fiber and adjacent to the interface are slightly different from the exact solution. Both the continuous condition along $y_3 = 0$ and discontinuous condition along $y_2 = 0$ are well captured by HFGMC and VAMUCH. The slight differences along the edges are caused by the interaction effects due to presence of adjacent cells because our far-field stress σ_{22}^{∞} is not really uniform along the edges which can be observed form the contour plot in Figure 2. It has been verified that if one chose a fiber volume fraction so low that σ_{22}^{∞} is uniform along the edges and the prediction of HFGMC and VAMUCH will be further improved. The discontinuity on the interface along $y_2 = 0$ in Figure 4 can be captured better if one refines the mesh in the vicinity. Although the effective properties are not sensitive to the discretization schemes, the local fields are. In this case, we used 100×100 subcells grid for GMC and HFGMC, and a mesh of 4834 8-noded quadrilateral elements is used for VAMUCH, and the same mesh is used for ANSYS to calculate G_{23}, and the corresponding 3D mesh is extruded from this mesh with two elements along the fiber direction to calculate all the other effective properties.

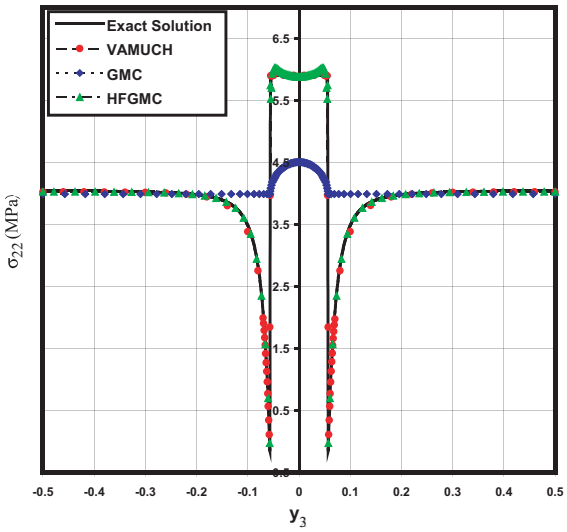

Figure 4. Comparison of normal stress σ_{22} distribution along $y_2 = 0$

B. Case 2: MOC microstructure

Next, we study a microstructure which is a square array with a square fiber in the center (Figure 6). We called it the MOC microstructure because it is typically used by MOC, GMC and HFGMC[6] We use the same boron fiber and epoxy matrix as the previous case. However, the fiber volume fraction is changed to be 60% so that the effective properties can be strongly affected by the fibers and their interactions with the matrix and with each other. The effective properties predicted by different approaches are listed in Table 2.

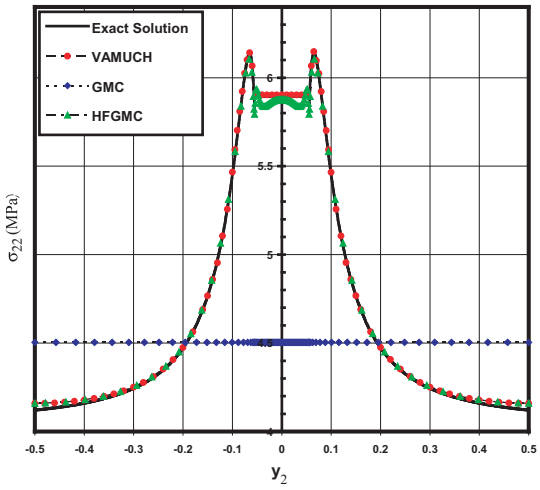

Figure 5. Comparison of normal stress σ_{22} distribution along $y_3 = 0$

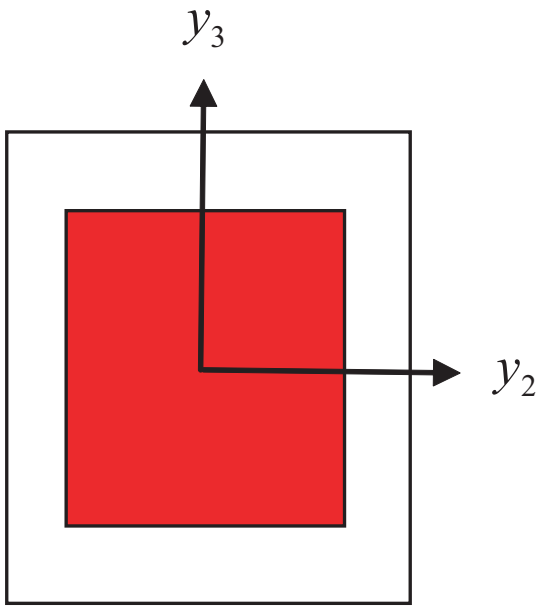

Figure 6. A sketch of the MOC microstructure

A 64×64 subcell grid is used for GMC and HFGMC, a 2×2 subcell grid is used for ECM, a mesh of 3763 8-noded elements is used for VAMUCH and the same mesh and its corresponding 3D mesh is used for FEM. It can be observed that only VAMUCH and FEM have the same predictions for all the effective properties, although all the approaches predict almost the same value for E_{11}, and HFGMC's predictions are very close to those of VAMUCH and FEM. Overall, GMC under predicts E_{22}, G_{12}, G_{23} and over predicts the Poisson's ratios. Except E_{11}, the predictions of ECM are located between GMC and HFGMC and close to those of HFGMC.

To evaluate the accuracy of the local stress field predicted by the different approaches, we use a plane strain problem by applying a biaxial loading such that $\sigma_{22} = -10$ MPa and $\sigma_{33} = 100$ MPa to the microstructure. We plot σ_{33} along $y_3 = 0$ predicted by different approaches in Figure 7, where ANSYS results are obtained by directly solving the plane strain problem without using the effective properties. It can be clearly observed that VAMUCH and HFGMC have excellent agreements with the direct finite element analysis of ANSYS, although the predictions of HFGMC are slightly off at the interface between fiber and matrix. It is also observed that the local field obtained using GMC, although much improved compared to those of case 1, are only predictive in an average sense. We have also compared other stress components and tested with other types of loading such as transverse shear and longitudinal shear, and similar trends have been found. Those results are not reported here for conciseness.

Table 2. Effective properties of boron/epoxy composites for MOC microstructure

Models	E_{11} (MPa)	E_{22} (MPa)	G_{12} (MPa)	G_{23} (MPa)	ν_{12}	ν_{23}
GMC	241422	17440	4631	3203	0.2522	0.2673
HFGMC	241428	19803	5216	3390	0.2501	0.2000
ECM (7th order)	241426	19793	5161	3368	0.2502	0.1994
VAMUCH	241426	19864	5223	3391	0.2501	0.1978
FEM	241426	19864	5223	3391	0.2501	0.1978

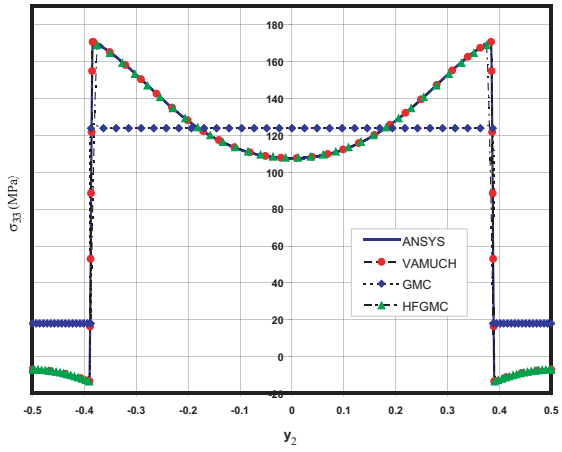

Figure 7. Comparison of normal stress σ_{33} distribution along $y_3 = 0$

C. Case 3: X microstructure

The last case we study is an X shaped microstructure, which is sketched in Figure 8, where each quadrant has two square fibers of the same size and equally spaced along the diagonal. The square fibers are perfectly connected with each other through the corners. The composite system considered is polymer-bonded explosives (PBXs) with an explosive crystal inclusion of Young's modulus $E = 15300$ MPa and Possion's

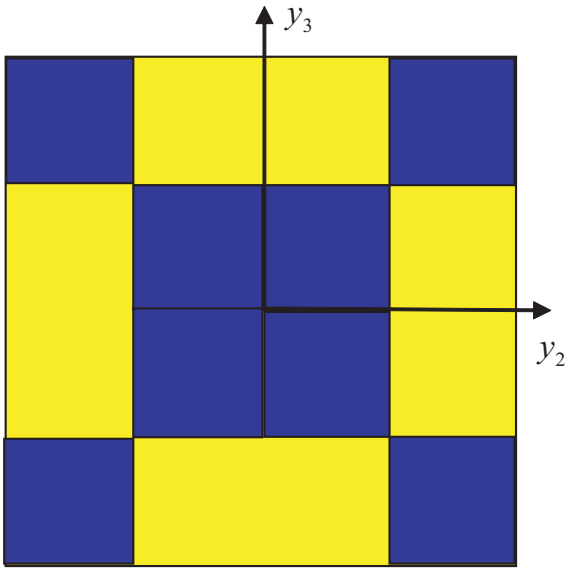

Figure 8. The sketch of X shape microstructure

ratio $\nu = 0.32$ embedded in a binding matrix with Poisson's ratio $\nu = 0.49$. To investigate the predictions from different approaches for different ratios of elastic moduli mismatches, we choose varying binding matrix material so that its Young's modulus E_m takes different values from 0.7 MPa, 7 MPa, 70 MPa, 700 MPa, and 7000 MPa. The fiber volume fraction is fixed at 50%.

Because of the special construction of this microstructure, singularities exist at all the connecting corners of the fibers. Even the calculation of effective properties becomes sensitive to the discretization schemes used by different methods. For this case, we used a 64×64 subcell grid for GMC and HFGMC, a 3×3 subcell grid is used for ECM, a mesh of 5712 8-noded elements is used for VAMUCH and the same mesh and its corresponding 3D mesh is used for the FEM. The effective properties with different Young's modulus for the binder predicted by different approaches are listed in Tables 3-7. We can observe the following from these tables:

- When $E_m = 7000$, all the approaches except GMC have excellent predictions for the effective properties. As shown in Table 3, GMC significantly under predicts G_{12} and G_{23}, slightly under predicts E_{11}, E_{22} and ν_{12}, and over predicts ν_{23}.

- For other values of E_m, the general trend is that when the contrast ratio of the Young's moduli of fiber and matrix becomes larger, the differences among the predictions from different approaches becomes larger, although all the approaches still predict a similar value for E_{11}, which approximately obeys the Voigt rule of mixture for fiber reinforce composites.

- For other values of E_m, VAMUCH and FEM also predict the same or similar value for E_{22} and Poisson's ratios. VAMUCH predictions for G_{23} are slightly larger than those of FEM predictions, while VAMUCH predictions for G_{12} are smaller than FEM and the difference become quite significant as the contrast ratio becomes large.

- For other values of E_m, the predictions of GMC, HFGMC, and ECM for E_{22}, G_{12}, G_{23}, although very different among themselves, are significantly lower than those of VAMUCH and FEM, while Poisson's ratios predicted from GMC, HFGMC, and ECM are bigger than those from VAMUCH and FEM. As the contrast ratio becomes larger, the difference between these two sets of results become much bigger.

- It is interesting to find out the GMC always predicts the same value for G_{12} and G_{23} for this microstructure for each value of E_m.

- The predictions of ECM are located between those of GMC and HFGMC for $E_m = 700$ MPa, 70 MPa and 7 MPa. However, such a trend is not present for $E_m = 7000$ MPa and 0.7 MPa. Particularly, for

Table 3. Effective properties of PBX 9501 composites for X microstructure ($E_m = 7000$ MPa)

Models	E_{11} (MPa)	E_{22} (MPa)	G_{12} (MPa)	G_{23} (MPa)	ν_{12}	ν_{23}
GMC	11150	10170	3343	3343	0.405	0.5212
HFGMC	11246	10530	3688	3794	0.4126	0.508
ECM (7th order)	11247	10546	3679	3804	0.4126	0.5072
VAMUCH	11247	10531	3690	3795	0.4126	0.5078
FEM	11246	10531	3690	3795	0.4126	0.5078

Table 4. Effective properties of PBX 9501 composites for X microstructure ($E_m = 700$ MPa)

Models	E_{11} (MPa)	E_{22} (MPa)	G_{12} (MPa)	G_{23} (MPa)	ν_{12}	ν_{23}
GMC	8000	1687	451.5	451.5	0.405	0.8687
HFGMC	8032	2544	1025	1406	0.4039	0.8032
ECM (7th order)	8024	2089	885.3	1314	0.4042	0.8382
VAMUCH	8041	2693	1207	1525	0.4036	0.7919
FEM	8040	2694	1213	1522	0.4036	0.7919

Table 5. Effective properties of PBX 9501 composites for X microstructure ($E_m = 70$ MPa)

Models	E_{11} (MPa)	E_{22} (MPa)	G_{12} (MPa)	G_{23} (MPa)	ν_{12}	ν_{23}
GMC	7685	182.5	46.79	46.79	0.405	0.9505
HFGMC	7690	376.2	153.2	277.3	0.3991	0.9037
ECM (7th order)	7688	233.7	112.1	214.4	0.4015	0.9387
VAMUCH	7701	798	553	715	0.3854	0.8232
FEM	7704	799	664	711	0.3853	0.8229

Table 6. Effective properties of PBX 9501 composites for X microstructure ($E_m = 7$ MPa)

Models	E_{11} (MPa)	E_{22} (MPa)	G_{12} (MPa)	G_{23} (MPa)	ν_{12}	ν_{23}
GMC	7654	18.41	4.696	4.696	0.405	0.9597
HFGMC	7654	40.16	18.43	33.96	0.3976	0.9197
ECM (7th order)	7654	23.67	11.53	23.00	0.4014	0.9503
VAMUCH	7658	502	468	569	0.3428	0.6839
FEM	7660	502	597	563	0.3425	0.6839

Table 7. Effective properties of PBX 9501 composites for X microstructure ($E_m = 0.7$ MPa)

Models	E_{11} (MPa)	E_{22} (MPa)	G_{12} (MPa)	G_{23} (MPa)	ν_{12}	ν_{23}
GMC	7650	1.842	0.4698	0.4698	0.405	0.9607
HFGMC	7650	4.058	4.123	6.367	0.3909	0.9277
ECM (7th order)	7650	0.3535	1.146	0.3178	0.4044	0.9925
VAMUCH	7651	460	459	553	0.3228	0.6223
FEM	7651	460	590	546	0.3228	0.6223

$E_m = 0.7$ MPa, the predictions of ECM for E_{22} and G_{23} are the lowest, while the method predicts the highest value for ν_{23}.

At this stage, we believe it is premature to conclude which sets of predictions are more reliable than others. First of all, it is impractical to connect two fibers through one material point (the corner). It is a mathematical idealization of small contacting areas. The singularity due to the stress bridging through the connecting corners creates difficult for all numerical approaches. Second, we are limited by resources to perform convergence studies for FEM results because its calculations except G_{23} requires 3D analysis. Although one would tend to blindly believe that the FEM results are the most reliable, this is not necessarily true. The reason is that even if all the results are converged, we have strong reasons to believe the assumed boundary conditions, particularly those applied for transverse shear and longitudinal shear, will significantly affect the results because of the extreme microstructural construction and contrast ratio of constituent properties.

Nevertheless, the aforementioned points by no means diminish the value of this case and the significance of the presented results. Due to its special construction and high contrast ratio, this case provides a great challenge to all micromechanics approaches. It clearly discloses the fallacy about micromechanics that every model "works" as far as effective properties concerned. This is a case worthy of the attention of the micromechanics community and more extensive research on issues such as convergence studies, size effects of the contacting areas, and even physical experiments, which are needed to make more authoritative conclusions.

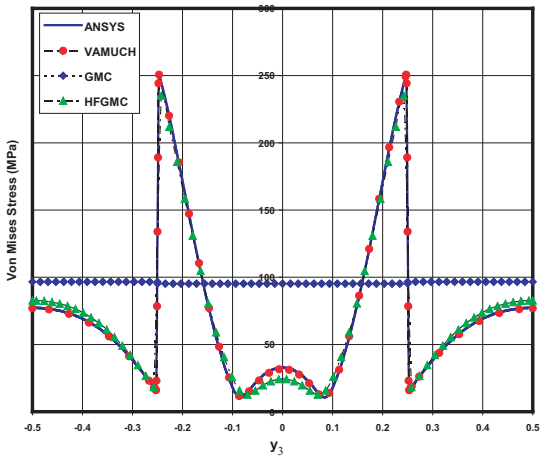

Figure 9. Comparison of von Mises stress distribution along $y_2 = 0$

Although the different approaches predict different effective properties, it is interesting to observe what happens in the predictions of local fields. Here we take the moderate case with $E_m = 700$ MPa to study a plane strain problem by applying a biaxial loading such that $\sigma_{22} = -10$ MPa and $\sigma_{33} = 100$ MPa to the microstructure. We plot the von Mises stress along $y_2 = 0$ predicted by different approaches in Figure 9, where ANSYS results are obtained by directly solving the plane strain problem without using the effective properties. It can be clearly observed that VAMUCH results are almost on the top of ANSYS results. HFGMC also has an excellent agreement with ANSYS although slight deviations have been found along the edges, fiber-matrix interfaces and the middle part of the microstructure. GMC predicts a uniform distribution which only provides an average prediction. To display the severe stress concentration around the connecting corner between inclusions, we provide a detailed contour plot around one corner in Figure 10. Indeed, stress concentration only happens in a very small area around the connecting point.

Conclusions

For the first time, several state-of-the art micromechanics models have been critically evaluated as a joint effort among the developers of these models. Such a comparison is valuable to researchers working to adopting a model to their particular applications or to understand what the current state of the art is in

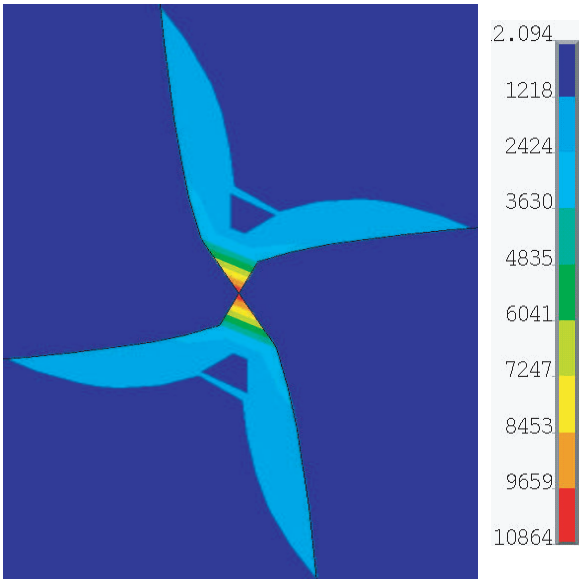

Figure 10. Contour plot of von Mises stress (MPa) distribution around a connecting corner

predictive capabilities in the field of micromechanics. Additionally the presented results (especially the local field predictions) will represent test cases for researchers seeking to determine the accuracy of the predictive capabilities of new micromechanics models. The X shape microstructure provides a very challenging test case for all micromechanics approaches, and more research is needed to pinpoint the real limits of the micromechanics approach in general, and various micromechanics models in particular.

Acknowledgements

The first author and last author would like to acknowledge the support of the National Science Foundation. The second author would like to acknowledge the support of the Los Alamos National Laboratory and the ASC program. The third and fourth authors would like to acknowledge the support of NASA Glenn Research Center.

References

[1]Jones, R., *Mechanics of Composite Materials*, Hemisphere, New York, NY, 1975.

[2]Herakovich, C., *Mechanics of Fibrous Composites*, John Wiley and Sons, New York, NY, 1998.

[3]Mori, T. and Tanaka, K., "Average Stress in Matrix and Average Elastic Energy of Materials with Misfitting Inclusions," *Acta Materialia*, Vol. 21, 1973, pp. 571–574.

[4]Benveniste, Y., "A New Approach to the Application of Mori-Tanaka's Theory in Composite Materials," *Mechanics of Materials*, Vol. 36, 1987, pp. 147–157.

[5]Williams, T. O., "A Generalized, Elasticity-based Theory for the Homogenization of Hetergeneous Materials with Complex Microstructures," 2007, in preparation.

[6]Aboudi, J., *Mechanics of Composite Materials: A Unified Micromechanics Approach*, Elsevier, New York, NY, 1991.

[7]Paley, M. and Aboudi, J., "Micromechanical Analysis of Composites by the Generalized Method of Cells," *Mechanics of Materials*, Vol. 14, 1992, pp. 127–139.

[8]Aboudi, J., "Micromechanical Analysis of Thermo-Inelastic Multiphase Short-Fiber Composites," *Composites Engineering*, Vol. 5, 1995, pp. 839–850.

[9]Aboudi, J., "Micromechanical Analysis of Composites by the Method of Cells - Update," *Applied Mechanics Reviews*, Vol. 49, 1996, pp. 127–139.

[10]Aboudi, J., "Micromechanical Analysis of Fully Coupled Electro-Magneto-Thermo-Elastic Multiphase Composites," *Smart Materials and Structures*, Vol. 10, 2001, pp. 867–877.

[11]Williams, T. O., "A Two-dimensional, Higher-oder, Elasticity-based Micromechanics Model," *International Journal of Solids and Structures*, Vol. 42, 2005, pp. 1009–1038.

[12]Williams, T. O., "A Three-dimensional, Higher-oder, Elasticity-based Micromechanics Model," *International Journal of Solids and Structures*, Vol. 42, 2005, pp. 971–1007.

[13]Nemat-Nasser, S. and Hori, M., *Micromechanics: Overall Properties of Heterogeneous Materials*, North-Holland, New York, NY, 1993.

[14]Bensoussan, A., Lions, J.-L., and Papanicolaou, G., *Asymptotic Analysis for Periodic Structures*, Elsevier, New York, NY, 1978.

[15]Yu, W., "A Variational-Asymptotic Cell Method for Periodically Heterogeneous Materials," *Proceedings of the 2005 ASME International Mechanical Engineering Congress and Exposition*, ASME, Orlando, Florida, Nov. 5–11 2005.

[16]Yu, W. and Tang, T., "Variational Asymptotic Method for Unit Cell Homogenization of Periodically Heterogeneous Materials," *International Journal of Solids and Structures*, Vol. 44, 2007, pp. 4039–4052.

[17]Yu, W. and Tang, T., "A New Micromechanics Model for Predicting Thermoelastic Properties of Heterogeneous Materials," *International Journal of Solids and Structures*, 2007, submitted.

[18]Sun, C. and Vaidya, R., "Prediction of Composite Properties from a Representative Volume Element," *Composites Science and Technology*, Vol. 86, 1996, pp. 171–179.

[19]Brockenbrough, J., Suresh, S., and Wienecke, H., "Deformation of Metal-Matrix Composites with Continuous Fibers: Geometrical Effects of Fiber Distribution and Shape," *Acta. Metall. Mater.*, Vol. 39, 1991, pp. 735–752.

[20]Brydon, A. D., Bardenhagen, S. G., Miller, E. A., and Seidler, G. T., "Simulation of the Densification of Real Open-Celled Foam Microstructures," *Journal of the Mechanics and Physics of Solids*, Vol. 53, 2005, pp. 2638–2660.

[21]Lissenden, C. and Herakovich, C., "Comparison of Micromechanical Models for Elastic Properties," *Space '92, Proceedings of the 3rd International Conference, Denver, CO*, Vol. 2, 1992, pp. 1309–1322.

[22]Pindera, M.-J. and Bednarcyk, B., "An Efficient Implementation of the Generalized Method of Cells for Unidirectional, Multi-Phased Composites with Complex Microstructures," *Composites: Part B*, Vol. 30, 1999, pp. 1009–1038.

[23]Bednarcyk, B. and Pindera, M. J., "Inlastic Response of a Woven Carbon/Copper Composite Part II: Micromechanics Model," *Journal of Composite Materials*, Vol. 34, 2000, pp. 299–331.

[24]Aboudi, J., Pindera, M.-J., and Arnold, S., "Higher-Order Theory for Periodic Multiphase Materials with Inelastic Phases," *International Journal of Plasticity*, Vol. 19, 2003, pp. 805–847.

[25]Aboudi, J., "Harmonic Waves in Composite Materials," *Wave Motion*, Vol. 8, 1986, pp. 289–303.

[26]Aboudi, J., "Transient Waves in Composite Materials," *Wave Motion*, Vol. 9, 1987, pp. 141–156.

[27]Aboudi, J., "Wave Propagation in Damaged Composite Materials," *International Journal of Solids and Structures*, Vol. 24, 1988, pp. 117–138.

[28]Aboudi, J., Pindera, M.-J., and Arnold, S., "Higher-Order Theory for Functionally Graded Materials," *Composites: Part B*, Vol. 30, 1999, pp. 777–832.

[29]Arnold, S., Bednarcyk, B., and Aboudi, J., "Comparison of the Computational Efficiency of the Original Versus Reformulated High-Fidelity Generalized Method of Cells," *NASA TM 2004-213438*, 2004.

[30]Aboudi, J., "The Generalized Method of Cells and High-Fidelity Generalized Method of Cells Micromechanical Models - A Review," *Mechanics of Advanced Materials and Structures*, Vol. 11, 2004, pp. 329–366.

[31]Bednarcyk, B. and Arnold, S., "MAC/GMC 4.0 User's Guide,," *NASA/TM-2002-212077*, 2002.

[32]Guedes, J. and Kikuchi, N., "Preprocessing and Postprocessing for Materials Based on the Homogenization Method with Adaptive Finite Element Method," *Computer Methods in Applied Mechanics and Engineering*, Vol. 83, 1990, pp. 143–198.

[33]Eshelby, J. D., "The Determination of the Elastic Field of an Ellipsoidal Inclusion, and Related Problems," *Proc. R. Soc. London A*, 1957, pp. 376–396.